# Polariton lasing vs. photon lasing in a semiconductor microcavity

**Hui Deng*†, Gregor Weihs*‡, David Snoke§, Jacqueline Bloch¶, and Yoshihisa Yamamoto*,**

*Quantum Entanglement Project, International Cooperative Research Project (ICORP), Japan Science and Technology Corporation, Edward L. Ginzton Laboratory, Stanford University, Stanford, CA 94305; ‡Institute of Industrial Science, Tokyo University, 4-6-1 Komaba, Meguro-ku, Tokyo 153-8904, Japan; §Department of Physics and Astronomy, University of Pittsburgh, 3841 O'Hara Street, Pittsburgh, PA 15260; ¶Laboratory of Photonic and Nanostructures, Centre National de la Recherché Scientifique, Route de Nozay, 91460 Marcoussis, France; and **NTT Basic Research Laboratories, Morinosato Wakamiya, Astugishi, 243-0198 Kanagawa, Japan

Edited by Paul C. Martin, Harvard University, Cambridge, MA, and approved October 29, 2003 (received for review July 10, 2003)

**Nearly one decade after the first observation of Bose–Einstein condensation in atom vapors and realization of matter-wave (atom) lasers, similar concepts have been demonstrated recently for polaritons: half-matter, half-light quasiparticles in semiconductor microcavities. The half-light nature of polaritons makes polariton lasers promising as a new source of coherent and nonclassical light with extremely low threshold energy. The half-matter nature makes polariton lasers a unique test bed for many-body theories and cavity quantum electrodynamics. In this article, we present a series of experimental studies of a polariton laser, exploring its properties as a relatively dense degenerate Bose gas and comparing it to a photon laser achieved in the same structure. The polaritons have an effective mass that is twice the cavity photon effective mass, yet seven orders of magnitude less than the hydrogen atom mass; hence, they can potentially condense at temperatures seven orders of magnitude higher than those required for atom Bose–Einstein condensations. Accompanying the phase transition, a polariton laser emits coherent light but at a threshold carrier density two orders of magnitude lower than that needed for a normal photon laser in a same structure. It also is shown that, beyond threshold, the polariton population splits to a thermal equilibrium Bose–Einstein distribution at in-plane wave number $k_{\|} > 0$ and a nonequilibrium condensate at $k_{\|} \sim 0$, with a chemical potential approaching to zero. The spatial distributions and polarization characteristics of polaritons also are discussed as unique signatures of a polariton laser.**

Experimentally realized macroscopic degenerate boson systems, such as lasers, superfluid $He^3$ and $He^4$, the Bardeen–Cooper–Schreiffer state in superconductors, and Bose–Einstein condensation (BEC) of atomic vapors, have deepened our fundamental understanding of macroscopic quantum orders and led to novel research tools as well as applications. A missing member from the family has been a macroscopically ordered state of weakly interacting bosons in condensed matter systems. Exciton and polariton BECs are the most promising candidates in this category. Since they were first proposed in the 1960s (1–3), tremendous efforts have been engaged in the search (4–13). Exciton and polariton BECs are attractive yet elusive because of the complications inherent to solid-state systems with strong Coulomb interactions. It is a formidable task to describe the excitations in solids in full detail. The common approach is to treat the stable ground state of an isolated system as a quasivacuum and to introduce quasiparticles as units of elementary excitation, which only weakly interact with each other. An exciton is a typical example of such a quasiparticle. As a result of optical excitation from the crystal ground state, an exciton consists of a bound pair of an electron and hole whose Coulomb interaction serves as the binding energy. Excitons have integral total spin, thus they behave like bosons, weakly interacting with each other through the residual Coulomb interactions of the fermionic constituents. The envelope wave function of an exciton is analogous to that of a hydrogen atom, in which an electron is bound to a nucleus. However, because of the strong dielectric screening in solids and a small effective mass ratio of the hole to the electron, the binding energy of an exciton in gallium arsenide (GaAs) is on the order of 10 meV (1 eV = $1.602 \times 10^{-19}$ J), three orders of magnitude smaller than that of hydrogen atoms, and the radius of an exciton is $\approx 10^2$ Å, extending over tens of atomic sites in the crystal. With the well developed techniques of molecular beam epitaxy, very high quality quantum confinement structures can be engineered. In a quantum well (QW) structure, excitons are confined inside a semiconductor layer with thickness comparable to the exciton radius, which restricts them to two-dimensional motion at low temperature. In GaAs, the lowest QW exciton states are split by spin-orbit interaction into two spin doublets, one $J = 1$ doublet that interacts strongly with the light field and one $J = 2$ doublet for which light emission and absorption are forbidden. When the GaAs QWs are placed at the antinodes of a semiconductor microcavity, the $J = 1$ exciton doublet strongly interacts with the optical field of the cavity, and new quasiparticles are formed called the upper polariton (UP) and lower polariton (LP) (14). The splitting between the UP and LP energies is determined by the number of QWs (15) and the coupling strength of the interband dipole moment to the cavity optical mode.

## Dynamic Condensation of Polaritons

As a linear superposition state of a cavity photon and a QW exciton, a polariton also obeys boson statistics at low densities. Hence, a BEC-type transition is expected when the correlation length of the LPs is comparable to or larger than the size of the system, which is determined by the spot size of the pump laser in real experiments (16). A conventional BEC exists in a thermal equilibrium system, where the particle lifetime is much longer than the relaxation time. However, the polariton condensation discussed here is dynamic in nature. The lifetime of the polaritons is shorter than or comparable to their energy relaxation time because of the leakage of their photonic components from the cavity. Hence, the polariton condensate is not in thermal equilibrium with its host lattice, and the phase transition is accompanied by emission of coherent light, which is analogous to an atom laser created out of an atom BEC. For this reason, we call the dynamic condensation of polaritons a "polariton laser."

In comparison with atom BECs, the dynamic condensation of microcavity polaritons occurs at a strikingly high temperature as a result of the mixing with cavity photons. Because of the dispersion of a cavity mode, cavity photons have an effective mass, but it is four orders of magnitude lighter than the exciton effective mass. A cavity mode and an exciton strongly couple to form polariton modes only when they have similar energies at the same in-plane wave vector $k_{\|}$. In the case that the photon mode is resonant with the exciton mode at $k_{\|} = 0$, a polariton in the $k_{\|} = 0$ state is half photon and

This paper was submitted directly (Track II) to the PNAS office.

Abbreviations: BE, Bose–Einstein; BEC, BE condensation; GaAs, gallium arsenide; QW, quantum well; LP, lower polariton; UP, upper polariton.

†To whom correspondence should be addressed at: Stanford University, 316 Via Paulo Street, Stanford, CA 94305. E-mail: dhui@stanford.edu.





www.pnas.org/cgi/doi/10.1073/pnas.2634328100

half exciton, with an effective mass $m_{pol}$ twice the photon mass, four orders of magnitude lighter than the exciton mass, and seven orders of magnitude lighter than the hydrogen atom mass. At the same time, the typical interparticle spacing, in units of the particle Bohr radius $a_B$, is $1/(n_{2D}^{1/2}a_B) \sim 10$ in polariton systems, much less than $1/(n_{3D}^{1/3}a_B) \sim 10^3$ in atom vapors. In other words, the density of polaritons in unitless numbers is generally much higher than that of atoms. Consequently, the critical temperature for polariton condensations is generally eight orders of magnitude higher than that needed for atom BECs. Room temperature dynamic condensation of polaritons in wide band gap semiconductors is not out of reach with present day techniques (15, 17).

The high density of polaritons also implies that interactions among them are more important than in atomic gases. This means that a polariton laser also offers a unique test bed for many-body physics theories. For example, when the quasiparticle density increases, a smooth transition from a polariton laser to a Bardeen–Cooper–Schreiffer-like state of excitons has been predicted for a system with low exciton decoherence rate (18, 19).

Another pronounced advantage of a polariton laser lies in the one-to-one correspondence between the polaritons and the photons emitted from the cavity. The photon component of a polariton has a fixed decay rate (normally on the order of 0.1 THz) out of the cavity. The emission of a photon preserves the polariton energy and in-plane wave vector. Therefore, the detected photons carry direct information of the polaritons. The intensity of the emission is proportional to the instantaneous polariton population, and the quantum statistical properties of the emission replicate those of the polaritons. Conversely, polaritons in certain momentum states can be selectively excited through resonant optical pumping.

## Experimental Principles

Because of the inherent complications of solid-state systems, observing the effect of polariton lasing requires careful attention to other nonlinear effects in the system. One example is coherent optical parametric amplification in a microcavity enhanced by polariton resonances (20–22). It is also based on the LP-LP scattering that originates from Columbic interaction between fermionic constituents, and there is also a nonlinear increase of coherent photon flux into the normal direction at $k_\parallel \sim 0$ LP energy. The gain in this case, however, is provided by coherent optical nonlinearities when both the pump and probe lasers are tuned to resonantly excite the $k_\parallel \sim 0$ polariton mode. The coherence of the $k_\parallel \sim 0$ state is directly inherited from the pump laser, analogous to the process of coherent four-wave mixing in nonlinear optics. In the present experiments, however, the pump laser excites polariton states at large $k_\parallel$, so that the coherence of the pump laser is lost by multiple phonon emission before the polaritons arrive at the $k_\parallel \sim 0$ states. The polaritons can only acquire macroscopic coherence by spontaneous symmetry breaking at the phase transition threshold. The coherence then is carried into the light field when the photon component of the polaritons leads to photon emission.

If the carrier density increases above a saturation density, the quasiparticle picture of polaritons breaks down, when induced transparency due to phase space filling reduces the exciton-photon coupling strength to the point that the LP-UP splitting is less than the line width. In this situation, the normal modes of the system become the cavity photon and the QW exciton. Further increase of the carrier density to above the electronic inversion condition leads to dissociation of the excitons into electron-hole plasma, and standard photon lasing takes place if the gain for the cavity photon mode exceeds its loss.

To realize polariton lasing before exciton saturation and transition to photon lasing requires appropriate engineering of the microcavity sample and efficient cooling of the hot-injected excitons. The molecular-beam-epitaxy-grown sample we used contains a $\lambda/2$ GaAs cavity sandwiched between $Ga_{0.8}Al_{0.2}$/AlAs distributed Bragg reflectors. Three stacks of QW are placed at the central three antinodes of a microcavity, each stack consisting of four 7-nm-thick GaAs QWs separated by-3 nm-thick AlAs layers. The microcavity thickness is tapered to allow tuning of the cavity resonance by changing the spot where the laser excites the sample. With a total of 12 QWs, the effective exciton density per QW is reduced to 1/12 of the total exciton density, suppressing the exciton density by an order of magnitude for a given polariton population. Moreover, the UP-LP splitting is increased by approximately the square root of the number of QWs (15, 23). Reflectivity measurements at 4 K showed a minimum UP-LP splitting of 14.9 meV. Because the splitting is comparable to the bare exciton binding energy of 10 meV, the effective size of the exciton component in the LP was predicted to be reduced dramatically (24). All these effects contribute to overcoming the saturation of excitons at high density.

In our experiments, the cavity mode was chosen to be resonant with the QW excitons at $k_\parallel = 0$, where their dipole coupling is maximum. The LPs have a dispersion relation:

$$E_{LP}(k_\parallel) = \frac{1}{2}[E_{exc} + E_c - \sqrt{(E_{exc} - E_c)^2 + 4\Omega}], \qquad [1]$$

where $E_{exc}$ and $E_c$ are the $k_\parallel$-dependent energies of the bare QW excitons and the cavity photon modes, and $\Omega$ is the collective dipole coupling strength, which in this case equals the splitting of $k_\parallel = 0$ LP and UP. Resonant optical pumping by mode-locked laser pulses is adopted to create instantaneously a population of exciton-like LPs at a large $k_\parallel$, so as to minimize the excitation of free electrons and holes, which usually increase the exciton decoherence rate. There are also indications recently that a large population of free electrons, however, may assist the energy relaxation of excitons (25–28). Dark $J = 2$ excitons, which are created by spin flip from the light-generated $J = 1$ excitons with a time constant of $\approx$100 ps (29), also may play a role. Injected exciton-like LPs relax by LP-LP scattering and phonon emission, thereby losing the coherence inherited from the pump wave and forming a real LP population with a quasithermal distribution. Phonon emission is sufficient to cool LPs at $k_\parallel \gg 0.1\, k_0$, where $k_0$ is the total wave number of the cavity photon at $k_\parallel = 0$. However, the process becomes very inefficient in the region $k_\parallel < 0.1\, k_0$, where the coupling between the cavity photon and the QW exciton becomes strong. In this region, as $k_\parallel$ decreases toward $k_\parallel = 0$, the effective LP mass is reduced from nearly the exciton mass to twice the photon mass, leading to a rapid decrease of the density of states of the LPs by four orders of magnitude. Furthermore, the lifetime of the LPs decreases from nearly the exciton lifetime of $\approx$500 ps to $\approx$4 ps. Consequently, most of the injected excitons decay radiatively before they relax to the bottom of the LP branch if only phonon emission is responsible for the cooling. The crucial process that efficiently cools LPs is the elastic scattering of two LPs into one near $k_\parallel = 0$ and one at higher energy. This process is enhanced by the bosonic final-state stimulation when the LP population per mode in the $k_\parallel \sim 0$ states exceeds unity (30). This stimulated LP-LP scattering is a phase-coherent process analogous to the stimulated emission of photons in a laser. Consequently, a macroscopic coherent population quickly can build up in the $k_\parallel = 0$ LP state, forming a polariton laser.

In all of our experiments, the sample temperature was 4 K. A mode-locked Ti-Sapphire laser (Coherent, Santa Clara, CA) with a pulse duration of 3 ps and a repetition rate of 76 MHz was used as the pump laser. The emitted light was collected with an angular resolution of 0.5° in air by using an optical fiber that was in turn connected to a charge-coupled device camera and imaging spectrometer or a streak camera for time-domain analysis. To measure the real-space polariton distribution, the LP emission was imaged onto a charge-coupled device camera by an aspheric microscope lens with a numerical aperture of 0.7. The lens was placed near the sample and aligned to the sample normal. In all measurements, the pump was either linearly or circularly polarized and focused to a

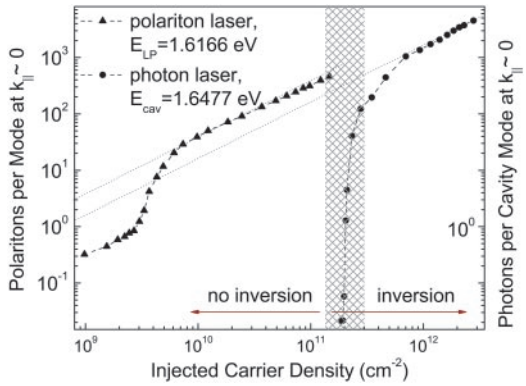


**Fig. 1.** Number of LPs and cavity photons per mode vs. injected carrier density for a polariton laser in scheme I (triangles) and a photon laser in scheme II (circles), respectively. The gray zone marks the population inversion densities from band edge to 15 meV above the band edge.

spot 15 $\mu$m in diameter at a position on the sample where the QW exciton was resonant with the cavity photon under weak excitation. At 45° from normal incidence in air, the pump was resonant with LPs having an in-plane wave number $k_{\parallel} = 5.33 \times 10^4$ cm$^{-1}$. At this incidence angle, direct coherent optical four-wave mixing is forbidden. We call this experimental condition scheme I. A scheme II was adopted to measure the phase transition of a photon laser in the same sample by using the same experiment setup. In scheme II, the pump laser was focused to a different position on the sample, where the cavity mode is blue-detuned to 15 meV above the band edge. The pump energy was tuned accordingly to be resonant with the cavity mode energy at $k_{\parallel} = 5.33 \times 10^4$ cm$^{-1}$.

## Threshold Carrier Densities

Phase transitions are observed in both schemes, as indicated by the sharp superlinear increase of the emission intensity into the normal direction with increasing pump intensity (Fig. 1). However, the critical carrier densities[††] are different by two orders of magnitude. In the polariton laser case (scheme I), the pump power density at threshold is $P_{\rm th} \sim 300$ W/cm$^2$, corresponding to an injected exciton density of $n_{\rm QW} = 3 \times 10^9$ cm$^{-2}$ per pulse per QW.[‡‡] It is about two orders of magnitude smaller than the Mott transition density ($n \sim 1/\pi a_{\rm B}^2$) and transparency condition of $10^{11}$ cm$^{-2}$ electron-hole pairs per QW. The LP population per mode around $k_{\parallel} = 0$ at threshold is estimated to be of the order of unity.[§§] This finding indicates that the nonlinear increase in the input–output relation in Fig. 1 originates from the onset of the stimulated scattering of LPs into the $k_{\parallel} \sim 0$ state.

[††]Here the critical density is defined where the nonlinearity is the largest in the input–output relation.

[‡‡]$n_{\rm QW}$ ($n'_{\rm QW}$) for polariton condensation (for photon lasing) is estimated from the number of pump photons per pulse ≈$5 \times 10^7$ (≈$6 \times 10^8$) multiplied by the net absorption of the microcavity system of ≈0.12% (≈2.3%) calculated by the transfer matrix method and divided by the number of QWs $N = 12$. For a spot of $D \approx 15$ $\mu$m in diameter, $n_{\rm QW} \approx 3 \times 10^9$ cm$^{-2}$ per pulse ($n'_{\rm QW} \approx 3 \times 10^{11}$ cm$^{-2}$).

[§§]LP population $n_{k\parallel} = 0$ at threshold is estimated to be ~1 by $N_{\rm LP} = n_{\rm LP} M \eta f_{\rm p} \Delta T_{\rm p} / \tau_{\rm LP}$ with the following parameters: the detected photon flux $N_{\rm LP} = 2{,}500\ s^{-1}$; the repetition rate of the mode-locked pump laser $f_{\rm p} = 76$ MHz; the overall detection efficiency $\eta \sim 10^{-4}$; the emitted pulse duration $\Delta T_{\rm p} \sim 10$ ps; LP lifetime $\tau \sim 4$ ps; and

$$M = \frac{1}{2}\frac{\pi D^2/4}{4\pi^2}\pi(k_0\Delta\theta)^2/4$$

is the number of transverse states subtended by the acceptance angle of the detector $\Delta\theta \sim 0.01$. $k_0 = 8.15 \times 10^4$ cm$^{-1}$ is the free space logitudinal wave number of the cavity photon. Cavity photon number per mode in $k_{\parallel} = 0$ is estimated in the same way, except that the cavity photon lifetime is ≈2 ps.

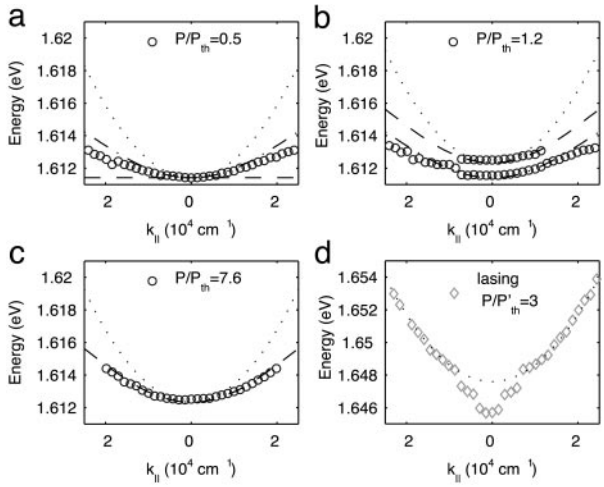


**Fig. 2.** Comparison of the measured and calculated dispersion curves. (*a–c*) Measured LP dispersion curves (circles) and calculated cavity photon (dotted line), unshifted LP (dashed-dotted line), and blue-shifted LP (dashed line) dispersion curves in scheme I, $P_{\rm th} = 300$ W/cm$^2$. Origin of the cavity photon dispersion is artificially shifted for comparison. (*d*) Measured (diamonds) and calculated (dotted line) cavity photon dispersion curves in scheme II, $P'_{\rm th} = 2$ KW/cm$^2$.

In the photon laser case, the injected carrier density at threshold is approximately $n'_{\rm QW} = 3 \times 10^{11}$ cm$^{-2}$ per pulse per QW,[‡‡] which is approximately the density required for electronic population inversion at 15 meV above the band edge. This result is in agreement with the standard laser mechanism. That is, the threshold of a semiconductor laser is solely determined by the electronic inversion condition if the active volume of the laser is large compared to its optical mode volume (31). The cavity photon number per mode is estimated to be of the order of unity again at threshold.[§§] This indicates that the nonlinear increase in the input–output relation originates from the onset of the stimulated emission of photons into the $k_{\parallel} = 0$ cavity photon mode.

## Dispersion Characteristics

To identify the normal modes of the above two nonlinear systems, we studied the energy vs. the transverse wave number by measuring the energy of the far-field emission at various external emission angles with an angular resolution of 0.5°. The dispersion curve measured for the polariton laser in scheme I agrees very well with the LP dispersion curve calculated with the transfer matrix method (Fig. 2 *a–c*). Below the polariton laser threshold, the energy of the LP photoluminescence is shifted slightly below the calculated dispersion curve (Fig. 2*a*) because of the Stokes shift of QW excitons. The shift is more noticeable at larger emission angles where the LP line width is wider because of an increasing portion of the exciton component and larger TE-TM splitting of the cavity modes (32). The blue shift of the whole dispersion curve with increasing pump rate reflects the exciton-polariton nonlinearities stemming from the Coulomb interaction and Pauli exclusion principle of the component fermions. As seen in Fig. 2 *b*, blue-shifted and nonshifted dispersions coexist. As discussed below, the spatial distribution of the polaritons changes abruptly at the threshold, leading to a high concentration of polaritons in the center of the laser spot, surrounded by a broad distribution of polaritons at lower density. We interpret the coexistence of the two dispersion curves as attributable to this spatial inhomogeneity. The blue-shifted dispersion corresponds to the central region and the nonshifted dispersion corresponds to the peripheral, nonlasing region. Well above the threshold, the nonshifted dispersion is no longer seen, because the intensity of the blue-shifted LP emission dominates the light emission (Fig. 2*c*). The measured dispersion follows unam-

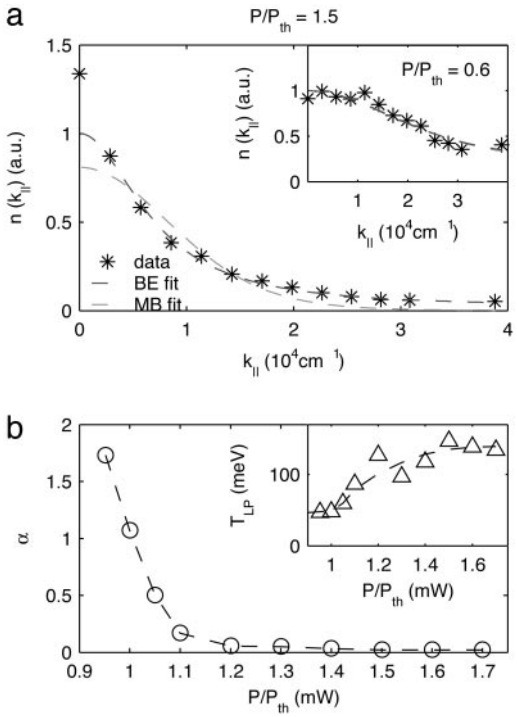


**Fig. 3.** Momentum space distribution of LPs. (*a*) The measured LP population per state vs. $k_\parallel$ (stars), compared with BE (solid line) and Maxwell–Boltzmann (dotted line) distribution functions at pump rates $P/P_{th} = 1.5$ and $P/P_{th} = 0.6$ (*Inset*). At $P/P_{th} = 0.6$, the fitted BE and Maxwell–Boltzmann distribution curves almost overlap. (*b*) The dimensionless chemical potential $\alpha$ vs. pump rate $P/P_{th}$ and the fitted effective LP temperature $T_{LP}$ vs. pump rate (*Inset*). The dashed lines are a guide for the eye.

biguously the calculated LP dispersion, which takes into account the blue shift of the excitons.

In scheme II (Fig. 2*d*), the measured dispersion curve agrees very well with the bare cavity mode dispersion except for a red shift of the lasing modes at $k_\parallel \sim 0$ attributable to the mode-pulling effect in semiconductor lasers (33). The emission energies are determined mainly by the cavity resonance, whereas the electronic population inversion with a maximum gain at a lower energy pulls the lasing energy slightly toward the gain maximum.

The difference in the dispersion characteristics shown in Fig. 2 *c* and *d* provides further evidence that the two nonlinear threshold behaviors seen in Fig. 1 correspond to the polariton lasing and photon lasing, respectively.

## Momentum Space Distribution

As reported in ref. 13, above the phase transition threshold in scheme I, a decrease of the second-order coherence function of the $k_\parallel \sim 0$ emission was observed, indicating the formation of macroscopic coherence in the LP condensate.

Another important aspect distinguishing the quantum state of polariton laser from a classical state is the momentum-space distribution of LPs. We converted the time-integrated intensity of the angle-resolved LP emission to the number density of LPs by taking into account the density of states and the radiative lifetime of LPs. In Fig. 3*a*, the LP number density vs. in-plane wave number $k_\parallel$ is compared with the classical Maxwell–Boltzmann distribution,

$$N(E) \propto \exp\left(-\frac{E_{LP}(k_\parallel) - E_{LP}(0)}{k_B T_{LP}}\right),$$

and the quantum mechanical Bose–Einstein (BE) distribution,

$$N(E) \propto 1 \Big/ \left[\exp\left(\frac{E_{LP}(k_\parallel) - E_{LP}(0) - \mu}{k_B T_{LP}}\right) - 1\right],$$

where the effective polariton temperature $T_{LP}$ and chemical potential $\mu$ are fitting parameters, and $k_B$ is the Boltzmann constant. The dimensionless chemical potential is defined $\alpha = (E_{LP}(0) - \mu)/k_B T_{LP}$. A lowest $k_\parallel = \Delta k \equiv 0.2 \times 10^4\ \mathrm{cm}^{-1}$ is used, corresponding to quantization in an area 15 $\mu$m in diameter, which is determined by the pump spot size. $\Delta k$ also corresponds to an experimental angular resolution of $\approx 0.3°$.

Below threshold, neither distribution fits the data well, probably because most of the polaritons decay radiatively before the system can reach thermal equilibrium (Fig. 3*a Inset*). Close to threshold, the BE distribution fits the data, with a fitted $T_{LP} \sim 50$ K and $E_{LP}(0) - \mu \sim -4.4$ meV, resulting in $\alpha \sim 1$. This marks the transition to a quantum degenerate gas. Also there is an extra peak above the thermal BE distribution appearing at $k_\parallel \sim 0$. This result implies that LPs start to accumulate in states with small $k_\parallel$, and hence the dynamic condensation of LPs is accelerated. Above threshold, surprisingly good agreement with a BE distribution is obtained, except for the extra population in the condensed $k_\parallel \sim 0$ state (Fig. 3*a*). $\alpha$ decrease rapidly near the threshold and reaches a minimum of $\alpha \sim 0.02$ at $P/P_{th} = 1.7$ (Fig. 3*b*). This finding demonstrates that the LPs form a degenerate Bose gas.

The fitted LP effective temperature $T_{LP}$ is higher than the lattice temperature of 4 K, and it increases with increasing pump rate (Fig. 3*b Inset*). This is because with increasing pump rate, energy relaxation of LPs is dominated by the efficient LP-LP scattering rather than the inefficient LP-phonon scattering, and therefore a quasiequilibrium is established among LPs before an equilibrium with the phonon reservoir can be established. The high effective temperature of the LPs implies that the polariton laser may survive at lattice temperatures higher than 4 K.[¶¶]

Far above threshold, the LP-LP interaction becomes strong. Therefore the condensate begins to be depleted, and the phase space filling of the excitons also becomes more severe. A BE distribution of free bosons is no longer appropriate to describe the experimental data; a theory for strongly interacting particles is needed in this regime.

## Relaxation Time vs. Polariton Lifetime

In accord with the observed quasithermal equilibrium of LPs near and above threshold, acceleration of the LP relaxation was seen in a time-domain spectral measurement. As shown in Fig. 4, when the pump rate increases beyond the threshold, the turn-on time of the emission at $k_\parallel \sim 0$ quickly drops to become comparable to the lifetime of the $k_\parallel \sim 0$ and $k_\parallel \sim 0.1\ k_0$ LPs, which are $\approx 4$ ps and 8 ps, respectively.

## Real Space Distribution

Complementary to the momentum space distribution, we have measured the real space distribution of the LPs (Fig. 5). A two-dimensional Gaussian profile of the LP population is observed below threshold with a full width at half maximum spot size $\omega \approx 15$ $\mu$m. Because of the steep incidence angle of the pump laser, the spot is slightly elliptical, i.e., wider along the pump incidence direction ($x$) and narrower along the orthogonal direction ($y$) (Figs. 5*a* and 6*a*). Close to threshold, a sharp peak emerges at the center of the spot, reducing the spot size to a minimum of $D_{min} = 3$ $\mu$m at $P/P_{th} \sim 1$ (Fig. 5*b*). Corresponding to such a small region, the far-field emission of the lowest-energy mode spreads over a region $|k_\parallel| \leq \pi/D_{min} \approx 1 \times 10^4\ \mathrm{cm}^{-1}$. This explains the flattening of the dispersion curve near $k_\parallel = 0$ at

[¶¶]Note that when $\alpha < 1$, the fitting of $T_{LP}$ bears a much larger error compared to $\mu$, because the total population is also a fitting parameter and the shape of the curve becomes rather insensitive to the temperature.

PHYSICS

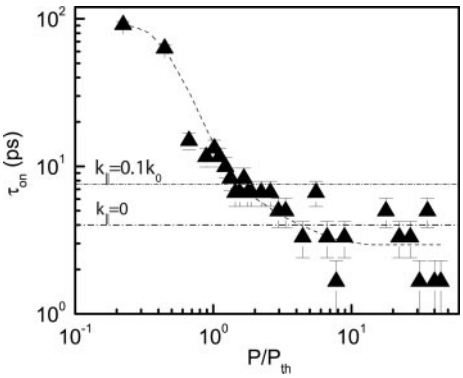


**Fig. 4.** Turn-on time $\tau_{on}$ of the emission at $k_{\|} \sim 0$ vs. pump rate $P/P_{th}$ (triangles) compared to the LP lifetimes at $k_{\|} = 0$ and $k_{\|} = 0.1\,k_0$ (dashed-dotted lines), where $\tau_{on}$ is defined as the delay of the maximum of the emission relative to the pump. It is derived from the time-domain spectral measurement after deconvolution of pump spectrum from the emission spectra. The dashed line is a guide for the eye.

$P/P_{th} \sim 1$, as observed in Fig. 2*b*. Because the emission from the whole area was collected in the measurements, the central condensed LPs and the peripheral noncondensed LPs explain the coexistence of two dispersion curves in Fig. 2*b*.

The spatial profile measured for a photon laser in scheme II also is reduced in size at the lasing threshold, with a minimum diameter of 7 $\mu$m. Because the spatial distribution of the electron-hole pairs determines the local gain, the region where the electron-hole density reaches the threshold value grows according to

$$\omega' = \omega_0 \sqrt{1 - \log_2(1 + P_{th}/P)}\,, \qquad [2]$$

where $\omega_0$ is an effective pump spot size including the carrier diffusion. Eq. **2** explains very well the increase of the measured lasing spot size in scheme II (Fig. 6*c*). Multiple transverse modes appear in the spatial profile (Fig. 6*b*), as is typical in large-area vertical cavity surface-emitting lasers.

In sharp contrast, the polariton laser maintains a uniform Gaussian profile up to very high pump rates, without obvious multiple transverse modes (Fig. 6*a*). The spot size expands remarkably slower than that predicted by Eq. **2**. This finding can be understood as follows. The LPs are delocalized and move ballistically over a distance of the order of microns before they decay radiatively. During their propagation, the LPs are selectively scattered into the $k_{\|} \sim 0$ state in the high-density region. Notice that the first sound velocity is not experimentally distinguishable from the group velocity of LPs, because of the relatively high kinetic energy of LPs compared to the interaction energy. For example, the group velocity of LPs is on the order of $10^4$ cm/s at $k_{\|} \sim 3 \times 10^4$ cm$^{-1}$ according to Eq. **1**, which is comparable to the sound velocity of LPs at threshold density estimated according to

$$v_s(n_{th}) = \sqrt{U_{int}(n_{th})/m_{LP0}} \sim 10^4 \text{ cm/s}, \qquad [3]$$

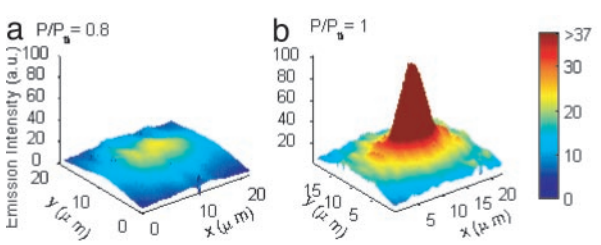


**Fig. 5.** Spatial profiles of LPs at $P/P_{th} = 0.8$ (*a*) and $P/P_{th} = 1$ (*b*).

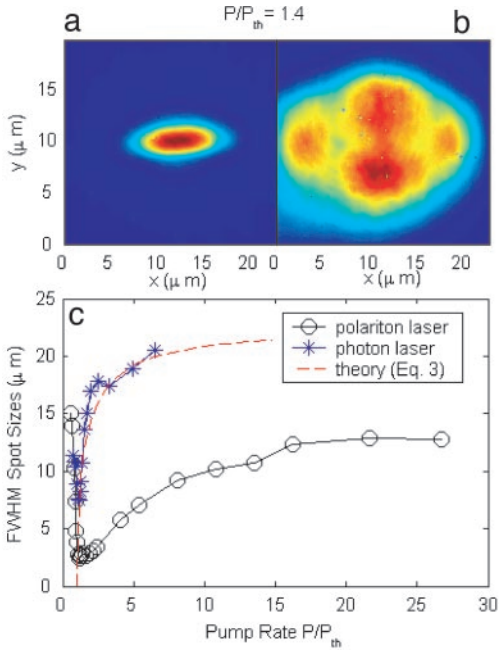


**Fig. 6.** The spatial profiles of LPs (*a*) and lasing cavity mode (*b*) at 1.4 times the threshold pump powers. (*c*) The expansion of the spot-size vs. pump rate for the polariton laser (circles) and the photon laser (stars). The latter fits well the transportless model described by Eq. **2** (dashed line) assuming a pump spot size of 23 $\mu$m.

where $m_{LP0} = 3.5 \times 10^{-5} m_e$ is the effective LP mass at $k_{\|} = 0$, and $m_e$ is the electron mass. The interaction energy at threshold is given by $U_{int}(n_{th}) = 6x(k_{\|} = 0)E_B a_B^2 n_{th}/(\pi D^2/4) \sim 0.7$ meV, with a threshold LP population of $n_{th} \sim 3.6 \times 10^{10}$ cm$^{-2}$, exciton binding energy $E_B \sim 10$ meV, exciton Bohr radius $a_B \sim 80$ Å, exciton fraction of the $k_{\|} = 0$ polariton $x(k_{\|} = 0) = 1/2$, and pump spot size $D \approx 15$ $\mu$m. A detailed dynamic model will be necessary to quantitatively describe the slow spatial expansion.

## Polarization Characteristics

As noted above, the pump laser is always either linearly or circularly polarized. A linearly polarized pump leads to a threshold pump power a factor of two smaller than that of a circularly polarized pump (Fig. 7 *a* and *b*). This is true for not only the polariton laser but also the photon laser. A straightforward interpretation follows from the fact that the cavity resonances are different for TE and TM polarized light, so that the linearly polarized pump light is more efficiently absorbed than the circularly polarized pump light.

By using a quarter-wave plate and a polarizer, we collected separately the left- and right-circularly polarized components of the emission, denoted as $\sigma_1$ and $\sigma_2$ hereafter. We define the degree of circular polarization $\eta = I\sigma_1 - I\sigma_2/I\sigma_1 + I\sigma_2$ to describe the difference between their intensities $I\sigma_1$ and $I\sigma_2$. According to the selection rule, the pump light with polarizations $\sigma_1$ or $\sigma_2$ excites the spin-up or spin-down LPs. Below threshold, the thermalization time is longer than the spin relaxation time. Hence, equal populations of spin-up and spin-down LPs are formed at $k_{\|} = 0$, and thus random polarization was observed regardless of the polarization of the pump. With increasing pump rate, the thermalization process is accelerated. Under the pumping of left-circularly polarized light, the LP population corresponding to $I\sigma_1$ accumulates faster than that corresponding to $I\sigma_2$, leading to an increase in $\eta$. As a result, stimulated LP-LP scattering and dynamic condensation occur first for copolarized LPs, $\eta$ escalating to larger than 0.9, as shown in Fig. 7*a*, whereas $I\sigma_2$ continues to grow linearly.

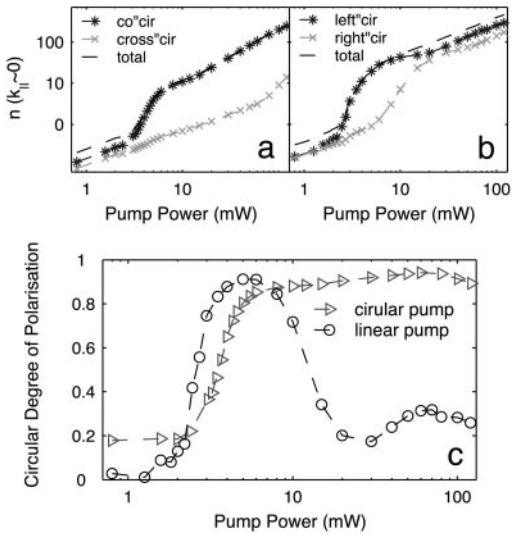


**Fig. 7.** Polarization properties of LP emission. Emission intensity of LPs near $k_{\|} = 0$ vs. pump power under circularly polarized pump (*a*) and linearly polarized pump (*b*). The two circular-polarization components of the emission and the their total intensities are plotted. (*c*) The circular degree of polarization vs. pump power with circularly polarized (triangles) and linearly polarized (circles) pumps.

Under the pumping of linearly polarized light, the initial spin-up LP population corresponding to $I\sigma_1$ was barely larger than $I\sigma_2$. Yet still $I\sigma_1$ rapidly overwhelms $I\sigma_2$ by spontaneous symmetry breaking when reaching the threshold $P_{\text{th}}$. At a pump density approximately three times $P_{\text{th}}$, the spin-down LP population corresponding to $I\sigma_2$ also reaches its threshold and increases nonlinearly. Resultantly, a fast increase of $\sigma$ around $P_{\text{th}}$ is followed by a sharp decrease around $3P_{\text{th}}$. The result indicates that spin-flip relaxation between LPs is slow compared to the stimulated LP-LP scattering. Therefore, the two kinds of LPs independently relax, condense, and decay. An alternative and more complicated explanation also may be possible. For example, in a rate equation model by Kavokin *et al.* (34), TE-EM splitting of LPs is taken into account, which causes coherent oscillation of circular polarizations in addition to the dephasing of the polarization because of LP-phonon scattering. The model also predicts a lower threshold for linearly polarized pumping and gives numerical results qualitatively in agreement with the data shown in Fig. 7.

## Summary

We have demonstrated experimentally that, with the increase of the pump intensity above a polariton laser threshold, the chemical potential of the BE distribution of the LPs approaches zero, whereas a narrow LP peak emerges at the $k_{\|} \sim 0$ state, consistent with a macroscopic condensation. The characteristics of the condensate are carried into the emitted photons and, hence, can be studied experimentally by measuring various aspects of the emission. Accompanying the polariton laser phase transition, there is a nonlinear increase of the emission intensity into the normal direction, an acceleration of the build up and decay of the emission, spatial concentration of the LPs followed by a slow expansion, and an increase in the degree of circular polarization. LP-LP scattering together with the bosonic final state stimulation plays the crucial role in cooling the injected hot excitons into the $k_{\|} \sim 0$ condensed state.

Quantitative analysis based on a many-body theory for the LP system will be necessary to understand the slow spatial expansion of the condensate and the quantum statistical properties of the condensate above threshold. A many-body theory based on fermionic Green's functions by Littlewood *et al.* (19, 35) treats the electrons and holes explicitly without introducing the bosonization of the excitons; hence, it can be applied to even the high carrier-density limit. It is predicted that with increasing carrier density, there is a smooth transition from a BEC-like state of LPs, which are defined as the elementary excitation of the system, to a Bardeen–Cooper–Schreiffer-like state of collective modes of the system, under the condition of low decoherence rate of electron-hole pairs. With further elaborations in the experimental techniques, this model may be directly tested by future experiments.

It is clear that polariton condensation has an advantage over a conventional semiconductor laser in terms of the energy efficiency. The threshold pump intensity of a polariton laser is one or two orders of magnitude lower than that of a photon laser. Moreover, it preserves a uniform single spatial mode even with a large pump spot size. Further research to create a polariton laser with electronic pumping and at room temperature may lead to a new source of coherent light.


1. Moskalenko, S. A. (1962) *Fiz. Tverd. Tela* **4,** 276–284.
2. Blatt, J., Brandt, W. & Boer, K. (1962) *Phys. Rev.* **126,** 1691–1692.
3. Keldysh, L. & Kozlov, A. N. (1968) *Sov. Phys. JETP* **27,** 521–528.
4. Lin, J. L. & Wolfe, J. P. (1993) *Phys. Rev. Lett.* **71,** 1222–1225.
5. Mysyrowicz, A., Benson, E. & Fortin, E. (1996) *Phys. Rev. Lett.* **77,** 896–899.
6. Dang, L. S., Heger, D., Andre, R., Boeuf, F. & Romestain, R. (1998) *Phys. Rev. Lett.* **81,** 3920–3923.
7. Senellart, P. & Bloch, J. (1999) *Phys. Rev. Lett.* **82,** 1233–1236.
8. Huang, R., Tassone, F. & Yamamoto, Y. (2000) *Phys. Rev. B* **61,** R7854–R7857.
9. Nagai, M., Shimano, R. & Kuwata-Gonokami, M. (2001) *Phys. Rev. Lett.* **86,** 5795–5798.
10. Huang, R., Yamamoto, Y., André, R., Bleuse, J., Muller, M. & Ulmer-Tuffigo, H. (2002) *Phys. Rev. B* **65,** 165314.
11. Butov, L. V., Gossard, A. C. & Chemla, D. S. (2002) *Nature* **418,** 751–754.
12. Snoke, D. (2002) *Science* **298,** 1368–1372.
13. Deng, H., Weihs, G., Santori, C., Bloch, J. & Yamamoto, Y. (2002) *Science* **298,** 199–202.
14. Weisbuch, C., Nishioka, M., Ishikawa, A. & Arakawa, Y. (1992) *Phys. Rev. Lett.* **69,** 3314–3317.
15. Saba, M., Ciuti, C., Bloch, J., Thierry-Mieg, V., Andre, R., Dang le, S., Kundermann, S., Mura, A., Bongiovanni, G., Staehli, J. L. & Deveaud, B. (2001) *Nature* **414,** 731–735.
16. Huang, K. (1995) in *Bose–Einstein Condensation*, eds. Griffin, A., Snoke, D. W. & Stringari, S. (Cambridge Univ. Press, New York), pp. 31–50.
17. Pawlis, A., Khartchenko, A., Husberg, O., As, D., Lischka, K. & Schikora, D. (2002) *Solid State Commun.* **123,** 235–238.
18. Comte, C. & Nozières, P. (1982) *J. Phys.* **43,** 1069–1081.
19. Szymanska, M. H. & Littlewood, P. B. (2002) *Solid State Commun.* **124,** 103–107.
20. Savvidis, P. G., Baumberg, J. J., Stevenson, R. M., Skolnick, M. S., Whittaker, D. M. & Roberts, J. S. (2000) *Phys. Rev. Lett.* **84,** 1547–1551.
21. Baumberg, J. J., Savvidis, P. G., Stevenson, R. M., Tartakovskii, A. I., Skolnick, M. S., Whittaker, D. M. & Roberts, J. S. (2000) *Phys. Rev. B* **62,** R16247–R16250.
22. Ciuti, C., Schwendimann, P. & Quattropani, A. (2001) *Phys. Rev. B* **63,** R041303–R041306.
23. Bloch, J., Freixanet, T., Marzin, J., Thierry-Mieg, V. & Planel, R. (1998) *Appl. Phys. Lett.* **73,** 1694–1696.
24. Khurgin, J. B. (2000) *Solid State Commun.* **117,** 307–310.
25. Ramon, G., Rapaport, R., Qarry, A., Cohen, E., Mann, A., Ron, A. & Pfeiffer, L. (2002) *Phys. Rev. B* **65,** 085323.
26. Malpuech, G., Kavokin, A., Carlo, A. D. & Baumberg, J. (2002) *Phys. Rev. B* **65,** 153310.
27. Tartakovskii, A. I., Krizhanovskii, D. N., Malpuech, G., Emam-Ismail, M., Chernenko, A. V., Kavokin, A. V., Kulakovskii, V. D., Skolnick, M. S. & Roberts, J. S. (2003) *Phys. Rev. B* **67,** 165302.
28. Lagoudakis, P., Martin, M. D., Baumberg, J. J., Qarry, A., Cohen, E. & Pfeiffer, L. N. (2003) *Phys. Rev. Lett.* **90,** 206401.
29. Snoke, D. W., Rühle, W. W., Köhler, K. & Ploog, K. (1997) *Phys. Rev. B* **55,** 13789–13794.
30. Tassone, F. & Yamamoto, Y. (1999) *Phys. Rev. B* **59,** 10830–10842.
31. Björk, G., Karlsson, A. & Yamamoto, Y. (1994) *Phys. Rev. A* **50,** 1675–1680.
32. Panzarini, G., Andreani, L. C., Armitage, A., Baxter, D., Skolnick, M. S., Astratov, V. N., Roberts, J. S., Kavokin, A. V. & Vladimirova, M. R. (1999) *Phys. Rev. B* **59,** 5082–5089.
33. Raja, M., Brueck, S., Scully, M. & Lee, C. (1991) *Phys. Rev. A* **44,** 4599–4607.
34. Kavokin, A., Malpuech, G., Lagoudakis, P. G., Baumberg, J. J. & Kavokin, K. (2003) *Phys. Stat. Sol.* **195,** 579–586.
35. Eastham, P. R. & Littlewood, P. B. (2001) *Phys. Rev. B* **64,** 235101.